Available on CMS information server

**CMS NOTE 2004/035**

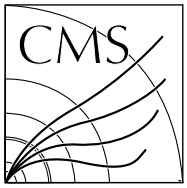


**The Compact Muon Solenoid Experiment**

# CMS Note

Mailing address: CMS CERN, CH-1211 GENEVA 23, Switzerland

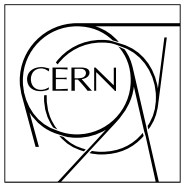


**January 6, 2005**

# CMS Silicon Tracker Module Assembly and Testing at FNAL

D. Coppage[1)], M. Demarteau[2)], C.E. Gerber[3)], W. Kahl[4)], E. Medel[5)], A. Ronzhin[2)], K. Sogut[2,a)], E. Shabalina[3)], L. Spiegel[2)], T. Ten[3)]

**Abstract**

This note is intended to provide details on a recent activity at FNAL in which CMS Tracker Outer Barrel modules were assembled and tested as part of a qualification of some of the sensor fabrication lines. At the same time the note serves to document the assembly and testing operations at FNAL for CMS silicon tracker modules.

Of the 88 modules produced for the qualification study at FNAL, one module was outside the mechanical alignment specification. For module bonding an introduced failure rate of $4.0 \times 10^{-4}$ faults per channel was observed. Eighty-five of the modules passed the full set of electrical tests. Two of the failures could be attributed to the sensors and one to a problem with the front-end hybrid. Additionally, a couple of the passed modules drew unusually high leakage currents. The high current modules are discussed in some detail.

[1)] University of Kansas, Lawrence, Kansas USA

[2)] Fermi National Accelerator Laboratory, Batavia, Illinois USA

[3)] University of Illinois, Chicago, Illinois USA

[4)] Kansas State University, Manhattan, Kansas USA

[5)] Facultad de Ciencias Físico Matemáticas, BUAP, Puebla, Mexico

[a)] On leave from Cukurova University, Adana, Turkey

# 1 Introduction

This note documents results from a recent exercise in which qualification silicon microstrip sensors fabricated by STMicroelectronics were assembled into CMS modules and tested at the Fermi National Accelerator Laboratory. Fermilab is one of two production sites for the U.S.CMS Si-Tracker project, which is responsible for the assembly for all of the modules in the CMS Tracker Outer Barrel [1] (TOB). The other production site is located at the University of California at Santa Barbara.

TOB modules consist of a carbon fiber support frame, a front-end electronics hybrid, and two approximately 10 cm by 10 cm silicon microstrip sensors. The sensors were fabricated by STMicroelectronics [2] (ST) in Catania, Italy. Detailed tests were performed on the sensors, and information about the depletion voltage and the number of bad strips was provided as input to the testing and assembly groups and taken into account while choosing sensors for a particular detector module, as described in section 2. Hybrids were manufactured and assembled in Switzerland and at CERN and shipped to FNAL for wirebonding and testing, as described in section 3. Hybrids and sensors that met our specifications were assembled into TOB modules by means of an automated module assembly system, as described in section 4. After assembly, the mechanical accuracy of the modules was corroborated (section 5), and modules were wirebonded (section 6). A technique was developed to reinforce modules to avoid damage during shipping, and this is described in section 7. Completed modules were subject to a series of tests developed to ensure their proper functionality at different operating temperatures. Tests were performed with a PC-based readout system (fast test) and using the full CMS readout chain (long term testing). The test results were also used to assign an electrical grade to the modules. Details of the testing procedure and electrical grading of completed modules are described in section 8. Additional description of the features observed for a small number of modules with pathological behavior is included in section 9.

Several U.S. and Mexican institutes are collaborating on the assembly of TOB modules. The production sites for this effort are located at FNAL and the University of California at Santa Barbara (UCSB). Between the two sites all 5,208 TOB modules plus spares will be assembled, tested, and eventually shipped to CERN for installation in the CMS experiment. In addition to TOB module production, both sites have agreed to bond and test a fraction of the Tracker End Cap (TEC) hybrids. TEC hybrids that are completed at UCSB are assembled into TEC modules at UCSB, whereas completed TEC hybrids at FNAL are shipped to TEC assembly sites in Europe. The production efforts at UCSB have been extensively detailed in a separate note [3]. It should also be acknowledged that most of the fixtures, plates, testing boxes, and tools described in this note were engineered and often times fabricated at UCSB.

Along with UCSB, we were asked to assemble and test modules using sensors provided by ST as part of an effort to formally qualify the ST production lines. This activity will be referred to in this note as the "qualification exercise". A similar exercise was undertaken by the TEC assembly and testing centers in Europe. In parallel, the CMS Quality Test Centers (QTC's) also probed a large number of ST qualification sensors as part of the same exercise.

Qualification sensors were received at FNAL in two separate deliveries, one in June and one in July of 2004. Module assembly began very soon after the sensors arrived as results were required in time for the July Tracker meetings. Due to the shortness of time, the second set was not processed as extensively as the first set. For example, all modules in the first set underwent a second round of fast testing following the long term testing, whereas repeat fast testing was done for only a few modules from the second set. All of the ST qualification assembly and testing work took place at the FNAL Silicon Detector Center (SiDet).

# 2 Sensor Pairing

In preparation for module assembly, a list of sensor pairs per anticipated module is produced using data stored in the CMS Tracker Database [4]. For the ST qualification exercise 176 ST sensors consisting of 90 layer 3-4 types (OB2) and 86 layer 5-6 types (OB1) were available for module production at FNAL. OB1 and OB2 sensors have 768 and 512 active channels, respectively. None of the qualification modules were stereo types as we did not have sufficient quantities of TOB stereo hybrids and stereo frames at the time.

A list comprising one sensor ID per line is input to a relay application provided to us by Valeria Radicci (University of Bari, Italy) for querying the CMS Tracker Database. For those sensors not reported as faulty, the output from this Sensor Query program reports the depletion voltage, the current at 450V bias, and the number and list of bad channels, as well as bad channels separately associated with four conditions: Idiel, Cac100, Rpoly, Istrip. Idiel flags strips with excessive dielectric leakage current caused by pinholes. Cac100 probes the effective coupling

capacitance at full depletion and at 100kHz, unmasking inter-strip shorts. Rpoly marks out-of-range polysilicon bias resistor values, and Istrip tests for excessive strip to backplane leakage current. The table below summarizes conditions for which a channel will be flagged [5]. Sensors designated as faulty in the Database are not considered further.

Table 1: Definition of bad channel conditions.

| DB name | Basic Accept Condition: | Wire Bond Status |
|---|---|---|
| Idiel | $I_{diel} < 1$ nA | Strip left unbonded |
| Cac100 | $Cac100 < 1.3$ pF/cm | Strip left unbonded (for contiguous group, all but 1st unbonded) |
| Rpoly | $1.0 < R_{poly} < 2.0$ MΩ | no change |
| Istrip | $I_{strip} < 100$ nA | no change |

Sensor ID's are then separated by type corresponding to either type OB1 or OB2 into two sets; each set is again separated into two further subsets of sensors by depletion voltage. Sensor depletion voltages below 200V define one subset of sensor ID's, and those above it define the second. Sensor pairs will only be made for sensors of the same type in the same depletion voltage range. This exercise, however, permitted one exception where one sensor with the highest depletion voltage in the low voltage set was paired with one sensor with the lowest depletion voltage in the high voltage set due to an odd number of members in each set.

After the division according to depletion voltage, another pairing pass is made to roughly even out the number of bad channels in a sensor pair. The algorithm proceeds by sorting the sensors according to the number of bad channels and folding the largest even set so that the sensor with least bad channels is paired with the sensor with the most bad channels. The rest follows in a similar manner. In all pairs, the sensor with the most channels to leave unbonded is selected for the outermost position (position 2) on the module. The output of the Sensor Query program permits extraction of the number and position of channels to be left unbonded and completes the prebuild information. Also at this time, new module ID's for these sensor pairs are registered, and the module components are virtually assembled in the Database.

Module ID's are 14 digit numbers chosen in accordance with the CMS Tracker barcode convention. However, for convenience in the following sections, module ID's will be abbreviated by the lowest order 4 digits. The table below shows the module ID's and sensor distribution for the two production runs that constituted the qualification exercise as well as some prebuild statistics.

Table 2: ST sensor qualification builds.

| | Module ID Range | OB1 Sensors | OB2 Sensors | No. Modules | Ave No. Strips To Be Left Unbonded | Ave. I(450V) |
|---|---|---|---|---|---|---|
| Set 1 | 7613-7633 | | 40 | 20 | 3.5 per module | 4.5 $\mu$A per module |
| | 7634-7656 | 48 | | 24 | | |
| Set 2 | 7657-7682 | | 50 | 25 | | |
| | 7683-7700 | 38 | | 19 | | |

The modules built for this exercise were TOB axial ($r$–$\phi$) modules for layers 3-4 and layers 5-6. Each module incorporates 2 sensors and a compatible hybrid on a common carbon fiber frame. The outermost sensor is bonded to one side of the inner sensor, which in turn is connected to APV (Analogue Pipeline Voltage) chips on the hybrid through a pitch adapter (PA). The APV readout chip handles 128 channels, so 4 are required for an OB2 module and 6 are required for an OB1 module.

# 3 Hybrid Wirebonding and Hybrid Thermal Testing

A critical component of a silicon detector module, besides the sensors of course, is the hybrid. The hybrids are manufactured at Cicorel, in Switzerland. After surface mounting of the readout chips and the passive components at Hybrid SA, also in Switzerland, the hybrids are shipped to CERN. At this stage there are three types of TOB hybrids. They are differentiated by the fact that 4 or 6 APV IC's are surface mounted. For the 4-chip hybrids the connector for data transmission can face the same side as the APV chip, called 'up', or the opposite side, called 'down'. At CERN the hybrid and pitch adapter (PA) are mounted on a 380 $\mu$m thick alumina substrate with a

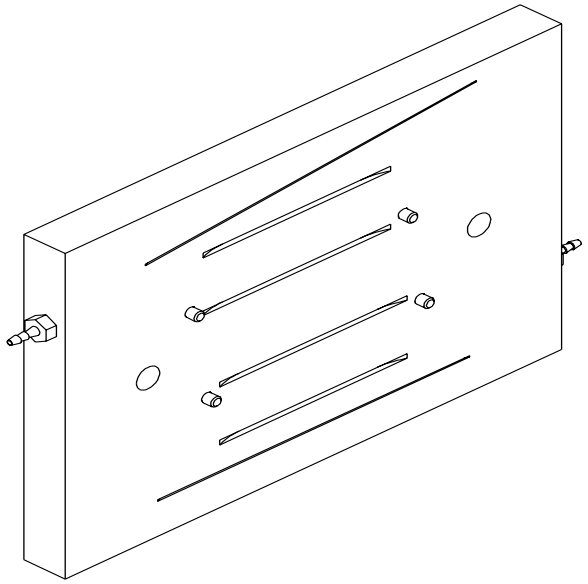

Figure 1: Drawing of the assembled wirebonding fixture.

50 $\mu$m glue layer. Since only layers 1 and 2 of the TOB have stereo readout, there is only one 4-chip stereo PA. There are thus five different hybrid types for the TOB: 4-chip axial and stereo, up and down, and 6-chip axial, up.

TEC Ring 2 and Ring 6 hybrids are also bonded and tested at Fermilab. Ring 2 has 6-chip hybrids with both axial and stereo PA's. All Ring 2 axial hybrids have the connector down, whereas all Ring 2 stereo hybrids have the connector up. Ring 6 has only 4-chip axial hybrids with the connector up. Each PA has slightly different dimensions. The hybrid wirebonding and testing thus has to accommodate a total of five axial hybrids and three stereo hybrids. To facilitate wirebonding, a single wirebonding fixture was designed that could accommodate all stereo hybrids and all TEC axial hybrids. Fig. 1 shows the drawing of the wirebonding fixture. Vacuum is provided through the sides. Rotating the fixture by 180 degrees changes its use from stereo to axial hybrid bonding. Fig. 2 shows a picture of the bonding fixture.

Hybrids assembled at CERN were shipped to FNAL, where the PA was bonded to the hybrid. This process included the wirebonding of the signal traces to the APV readout chip as well as a connection for the bias ring of the inner sensor. Following CMS recommendations, five wire bonds were placed for the bias connection. The wirebonding process utilizes a Kulicke & Soffa Industries model 8090 wirebonder [6] programmed to automatically wirebond a hybrid once it has been aligned on the machine.

A total of 640 hybrids of five different types have been wirebonded and thermally tested at FNAL. For the qualification exercise, 45 4-APV hybrids and 13 6-APV hybrids were bonded and tested at FNAL, whereas 30 6-APV hybrids were received from UCSB already bonded and tested, but were retested with the APV Readout Controller (ARC) [7] system at FNAL. At the time of the exercise, there was evidence of open via's on a fraction of the Tracker hybrids. To minimize the likelihood of encountering such cases, we were instructed to use hybrids only from two specific batches: 040312_TOB4PU and 040407_TOB6PU.

The project specifications require that the individual bond pull strengths exceed 9 grams. The strength of the wire bonds for each hybrid was verified on the test pads of the PA using a Dage BT-14 pull tester [8] at the start of the project. As our confidence in the wirebonding increased, only every tenth hybrid was checked. Fig. 3 shows the clean room at FNAL where the wirebonders are installed.

After the hybrid has been wirebonded it is inspected visually and sent on to the hybrid thermal test. The system and software used for this test were originally designed and developed by CERN and Aachen. The objective is to test the silicon electronics, to locate open and shorted channels on the hybrid, and to determine whether the hybrids will fail to read out at $-10°$C, the normal operating temperature for the Tracker system.

The thermal hybrid test setup has an integrated peltier element as main temperature regulator at its core. A Neslab RTE-140 chiller with a 40% ethylene-glycol water mixture running at a temperature of $3°$C provides the cooling for the peltier element. Four positions are provided on the base plate for the testing of hybrids. The hybrids are mounted on special aluminum carrier plates, and these plates are positioned on one of the four stations on the base plate. Separate carrier plates were designed at FNAL for axial and stereo hybrids. Each position can accommodate

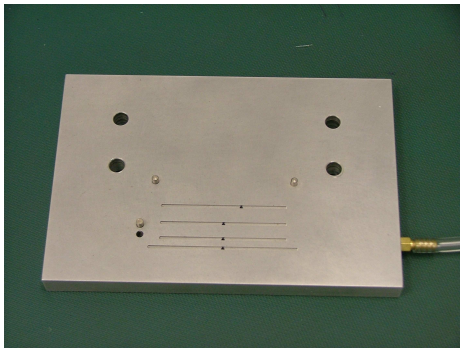

Figure 2: Hybrid bonding fixture.

Figure 3: The K & S 8090 wirebonders at FNAL.

both axial and stereo hybrid types. During the electrical test, the base plate is covered with an aluminum cover to create a lightight and airtight volume. Dry air is circulated through this volume to avoid condensation when the hybrids are tested at low temperature. The base plate is equipped with temperature and humidity sensors that are read out during the testing. A pair of relays controls the current polarity of the peltier element to set the tester in heating mode, cooling mode, or to switch it off. Fig. 4 shows the thermal test set up at FNAL and Fig. 5 shows the test box with four hybrids mounted.

A thermal cycle for the hybrids consists of three identical electrical tests: one at room temperature before cooling, one after cooling to $-20°$C, and a final test after returning to room temperature. At each temperature a standard set of electrical tests is run checking the pedestal, noise, and pulse shape distributions. Open, shorted and noisy channels are identified in this test. When a signal at the input of one of two channels is split with a neighboring channel by using the internal calibration of the APV chip, it is identified as a short. The existence of open channels is determined by the output of the pedestal distribution. Communication between the hybrid and the readout electronics is also verified at low temperature.

During thermal cycling, the hybrids are read out with the ARC system. The analogue signals from the APV chips are digitized with an 8-bit FADC. Two hybrids are connected to one ARC board *(single board setup)* via one 26 conductor twisted pair flat cable. The ARC board provides all communication with the hybrid. Two separate LabVIEW [9] applications provide graphical interfaces for the electrical tests and operating controls. During different phases of hybrid testing APV frames, pedestals, noise, gain, and hybrid current and voltages are displayed.

During the qualification exercise at FNAL, we were able to test 48 hybrids per day, with the entire process taking approximately 45 minutes per each set of 4 hybrids. The results obtained for TOB hybrids are in good agreement with results reported by other testing centers [3]. At Fermilab, 96% of the hybrids passed the thermal cycle test based on the number of noisy and open channels and were given a grade A or B. For TEC and TOB hybrids with 4 APV's, a hybrid is classified as grade A if it has 0-2 noisy or open channels and grade B if it has 3-4 noisy or open channels. These ranges are increased to 0-3 and 4-6 channels, respectively, for the 6-APV TEC and TOB hybrids. In case a hybrid can not be classified into these two categories due to excess problem channels, it is assigned a failing grade. The results from the hybrid testing were stored in the CMS Tracker Database via an XML file, which is generated by the testing software.

# 4 Gantry

Use of an automated module assembly system by CMS was motivated by the need for building some 20,000 modules in a uniform fashion at multiple assembly centers[1)]. The prototype robotic assembly system was developed at CERN [10] based on the Aerotech AGS 10000 gantry system [11]. The Fermilab gantry is essentially the same as the CERN and other gantry systems, but has been uniquely configured to assemble TOB modules. This system provides motion in four coordinates (three linear and one rotational) and is shown in Fig. 6. The linear and rota-

[1)] Module assembly centers include Bari, Brussels, FNAL, Lyon, Perugia, UCSB, and Vienna. The CERN gantry is used for assembling hybrids.

Figure 4: Hybrid thermal test setup.

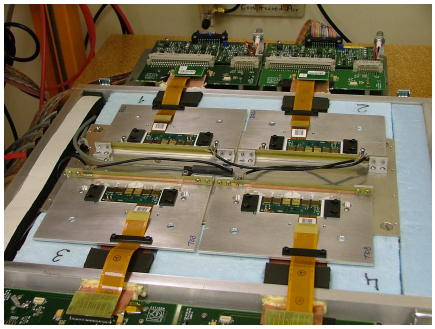

Figure 5: Test Box with 4 TEC 4-APV hybrids.

tional motors are controlled by a dedicated PC running an Aerotech MMI (Man Machine Interface) application. Software, initially developed at CERN, controls the assembly process including the initial survey of module parts, gluing operations, pick and placement of parts, and the final survey of the assembled modules.

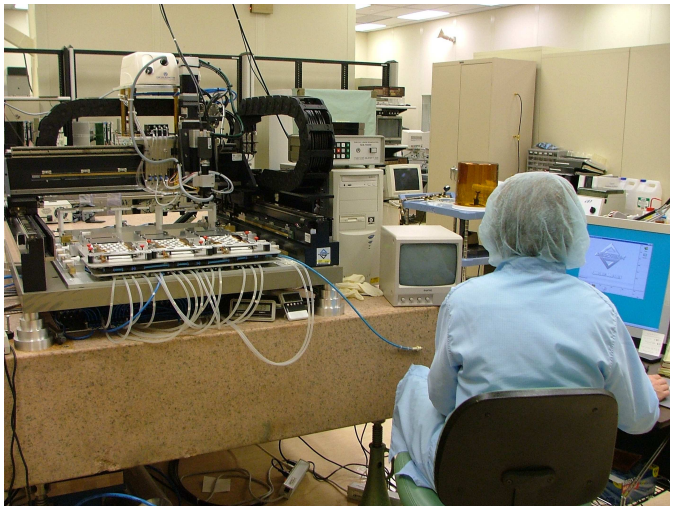

Figure 6: The FNAL gantry inside the clean room.

Surveying of module components is performed through the use of a CCD camera mounted on the $z$ axis of the gantry (see Fig. 7). The output of the camera is introduced to LabVIEW IMAQ pattern recognition software via a National Instruments PCI-1409 frame grabber card. This allows the accurate measurement of fiducial markers on the sensors and PA's.

An air pressure and vacuum system, very similar to what was developed for the CERN gantry, is used to pick and place module components and to hold them in place. Both air pressure and vacuum is available in the assembly clean room and is distributed to the gantry via a system of reservoirs, Festo [12] electromechanical valves, and sensors. The valves and sensors are controlled by a custom digital IO interface box connected to TTL level channels provided on the Aerotech U600 and 4EN-PC ISA cards.

Assembly plates are module type specific. For TOB module assembly two plates are required: an axial plate and a stereo plate. These two assembly plate designs are shown in Fig. 9 and Fig. 10. The assembly process for both types of TOB modules differs only in the method used to hold the module frames. The stereo assembly plates

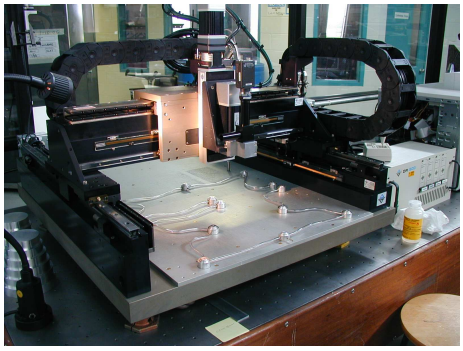

Figure 7: Pattern recognition camera mounted on the $z$-axis along with $\theta$ motor.

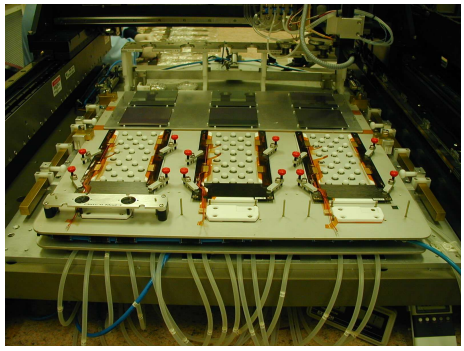

Figure 8: Gantry supply and assembly plates.

hold the module frame in a position rotated by the 0.1 radian stereo angle. In both cases, the sensors are moved from the storage plate to the assembly plate in a straight line with only a small rotational correction applied due to misalignment of the sensors on the supply plate or a misalignment of the frames on the assembly plate.

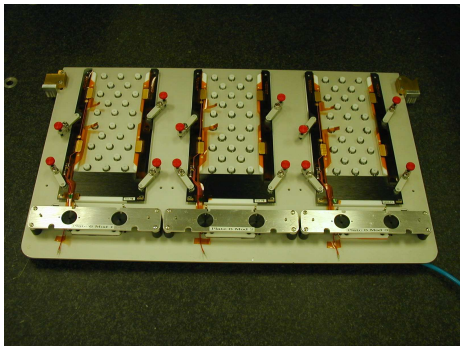

Figure 9: TOB axial assembly plate.

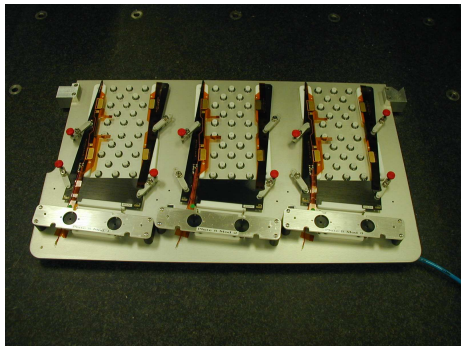

Figure 10: TOB stereo assembly plate.

The assembly process requires various tools for moving module parts and gluing operations. These tools are stored on a rack accessed by the gantry during the assembly process. Fig. 11 shows the tool rack with the different tools necessary for assembly of both types of TOB modules. Placement of the hybrids on the module occurs during one of the last steps in the assembly process. They are held on the assembly plate under vacuum by the hybrid bridge. The bridge serves not only as holding fixture but also as a pick-up tool for the transfer of the hybrid from the storage position to the module frame. The bridge is shown in Fig. 12.

To calibrate the gantry systems several glass plates with optically surveyable grids were prepared by CMS collaborators in Catania, Italy. Along with UCSB we shared a single plate with a 2 cm $\times$ 2 cm survey grid. At FNAL the Catania plate markers were initially measured using an OGP (Optical Gauge Products) Avant 400 optical inspection system [13]. The OGP has an accuracy of about 2-3 microns over the area of the measured plate. The Catania plate was then measured by the gantry pattern recognition system and the two sets of measurements compared. In the gantry $x$ direction (toward the operator) the differences are less than 10 microns. However, the gantry $y$ differences are as large as 100 microns toward the end of the $y$ range. Plots of the differences are shown in Fig. 13. Based on the differences a 2D correction file was produced, which yields, on average, positioning of sensors to an accuracy of around 4-5 microns. The use of glue, necessary for the physical assembly of modules, degrades this by about another 3 microns.

Two technicians participate in the module assembly, and it takes approximately one hour to build a set of 3 TOB modules. Generally the components (carbon fiber frame, hybrid, and two sensors) have been set aside in advance.

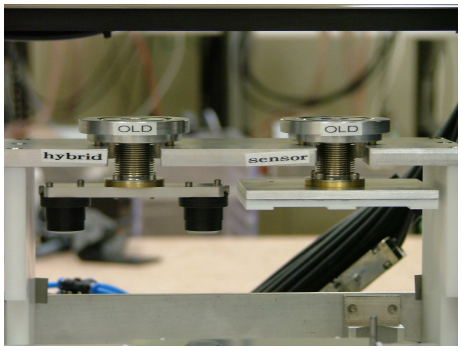


Figure 11: Photo of the hybrid (left) and sensor (right) pick-up tools on the gantry tool rack.

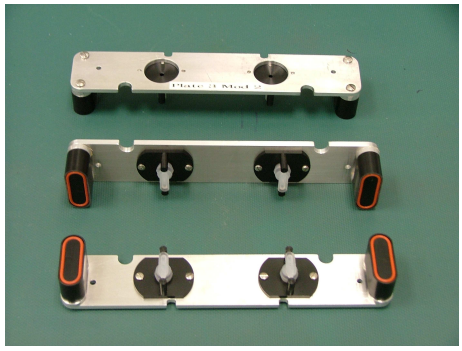

Figure 12: Photo of the bridge used in picking up the hybrid.

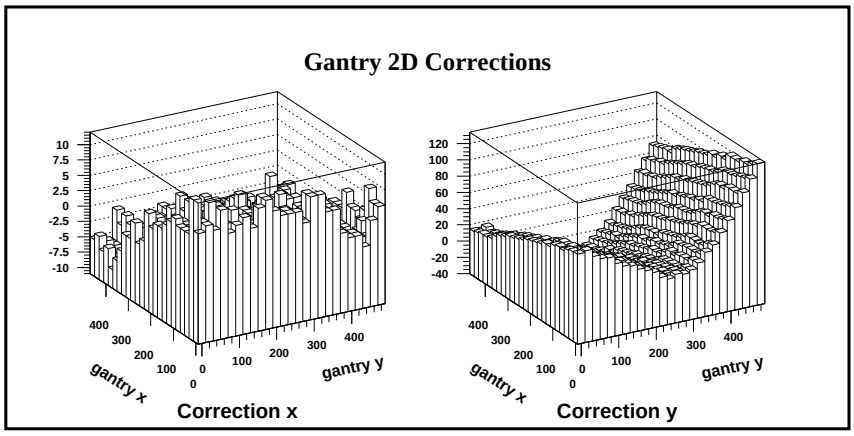


Figure 13: 2D mapping of the gantry precision in $x$ (left) and $y$ (right) before calibration. The horizontal scale units are in millimeters and the vertical scales in microns.

In addition to the gantry operations, the assembly time also includes a visual inspection of the sensors, scanning the sensor and hybrid barcodes, and documentation.

Three sets of carbon fiber frames are loaded on an assembly plate in preparation for module construction. The frames are located by pairs of precision pins, which are attached to the assembly plate. For each plate the positions of the pins relative to the plate markers are known, and the pins are not remeasured during the assembly process. The predicted coordinates of the pins in the gantry system are used to define a *frame* system for each module; ignoring small rotations, the relationship between the two systems is that the *frame* $x$-axis is in the same direction as the gantry (negative) $y$-axis and the *frame* $y$-axis is in the same directions as the gantry (negative) $x$-axis.

Sensors are loaded onto the supply plate using a transfer frame, and frames and hybrids are placed on the assembly plate. The transfer frame insures that the sensors are adequately pre-positioned for pattern recognition. Once vacuum is established for the supply and assembly plates and the sensors, the camera establishes the positions of the component markers. While one technician operates the gantry a second technician prepares the glues and loads these into syringes that are placed on the tool rack. Module assembly requires three different glues: Dow Corning 3140 for adhering the sensors to the frame, GE RTV12 (stiffened with glass beads) for mounting the hybrid to the frame, and Tra-Con TRA-DUCT silver epoxy for establishing the bias connection to the back of the sensors. The sensor tool is used to move the sensors, and this is followed by the use of the hybrid tool for transferring the hybrid/bridge combinations. After all assembly operations are complete a camera survey is made of the component markers. Vacuum is then switched from the gantry to an external source and the assembly plate removed from the gantry and placed in a curing box (shown in Fig. 14). Assembly plates remain in the curing box, under vacuum, until the next morning.

Figure 14: The cabinet used to store the modules during glue curing.

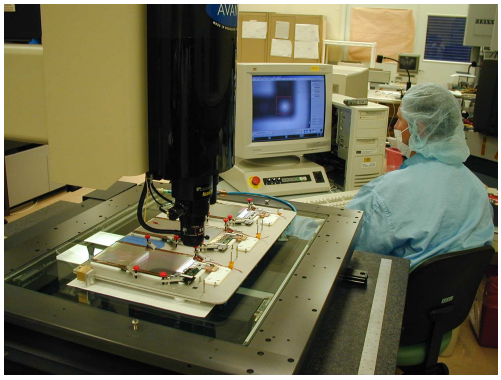

Figure 15: The OGP microscope measuring a plate of assembled modules.

To assess the accuracy of the FNAL gantry, we looked at the results from the 88 qualification modules. The most critical parameters to look at in module construction are the placement of sensors on the frame, mutual offset between the two sensors, and the relative angle between the sensors. The placement accuracy of the sensors on the module frame is determined by looking at the coordinates of the left markers on each sensor. Fig. 16 shows the *frame* system $x$ and $y$ coordinates of markers 1 and 3 for the sensor closest to the PA. Since the sensor strips run in the $y$ direction, sensor offsets in the $x$ direction are critical both for physics and for wire bonding reasons. Fig. 17 shows the difference between the $x$ position of marker 3 of the inner sensor and the $x$ position of marker 1 of the outer sensor. The angular difference between the two sensors is shown in Fig. 18.

Modules are graded based on the difference between measured and nominal values. For *frame* system $x$ and $y$ measurements, a module is considered grade A if all differences are within $\pm 30$ $\mu$m, and grade B within $\pm 39$ $\mu$m. Similarly, the sensor angles and the relative angles need to be within $\pm 10$ millidegrees for grade A and $\pm 13$ millidegrees for grade B. Out of the 88 qualification modules 85 were grade A, two grade B, and one was out of tolerance.

# 5 Optical Inspection

It takes about ten minutes per assembly plate to measure the post-cure position of the sensors and hybrids on the gantry. In order, though, to have the gantry immediately available for production at the start of each day, we have explored the use of the same OGP system described in the previous section for the post-cure measurements. That is, during the qualification exercise assembly plates with cured modules were first measured on the gantry and then moved to the OGP for a second set of measurements. Although gantry-generated XML files were uploaded to the Tracker Database during the exercise, we cross-checked the gantry results with OGP measurements. Fig. 19, for example, shows the difference between the relative sensor angles as measured on the gantry and on the OGP. Results from the comparison studies have been used to determine offset parameters for the gantry assembly process, with the goal of better centering OGP residual distributions in future production efforts.

The main reason for using the OGP for post-cure measurements is to save time in the production process. However, the OGP also has a significantly higher measurement accuracy than the gantry. Over the range of an assembly plate, for example, the OGP accuracy is around 2-3 microns whereas the corresponding gantry accuracy is around 4-5 microns. One of the limiting features for the gantry are the large $y$-direction corrections—as large as 100 microns—in particular regions of the active area. By checking the known distance between markers on the same sensors, for example, we know that the gantry 2D file could be improved in the assembly plate module-one position. However, this would require a finer calibration grid than what was used to generate the 2D file.

Fig. 15 shows an assembly plate on the OGP inspection table. As in the gantry post-cure measurement, the sensors and hybrids are no longer under vacuum. Also, as in the gantry measurements, the assembly plate markers are used to calculate the location of the precision pins. The OGP measurements begin with the operator manually locating the two markers. The left marker is used to define an origin and the right marker to establish an $x$–$y$ coordinate system. Once the origin and axes have been determined the actual measurement of module fiducial marks is largely

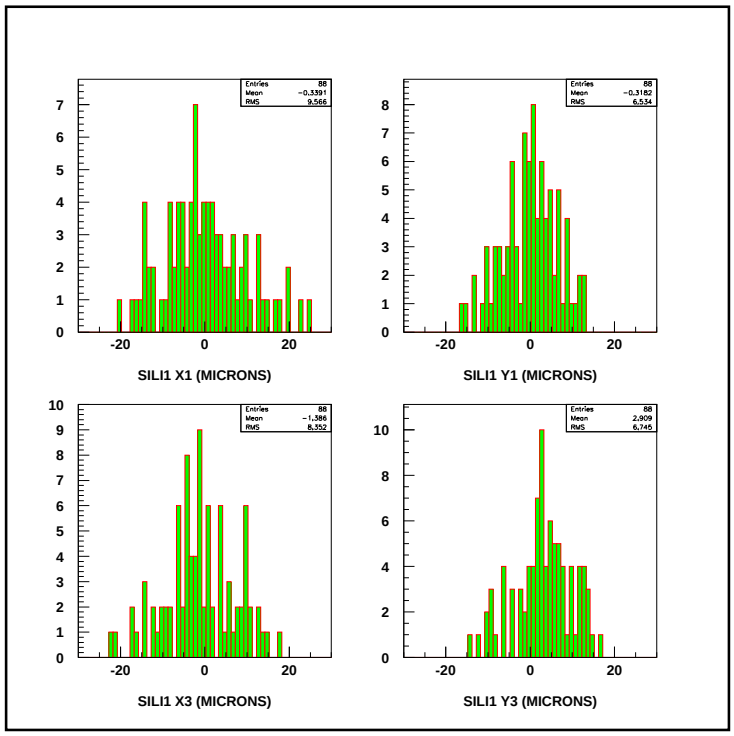


Figure 16: *Frame* $x1$ and $x3$ positions for inner sensors.

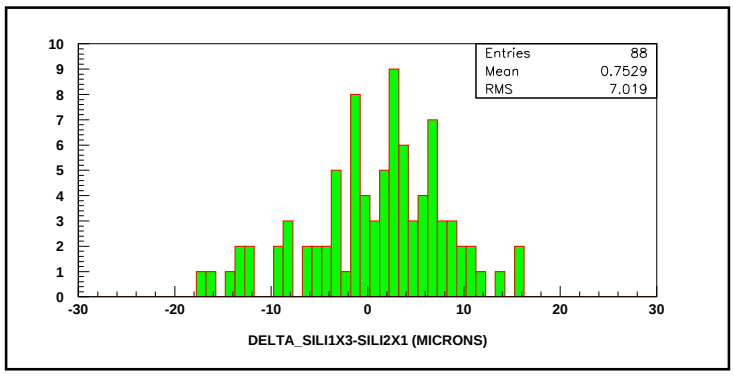


Figure 17: Difference in $x$ positions between inner and outer sensors.

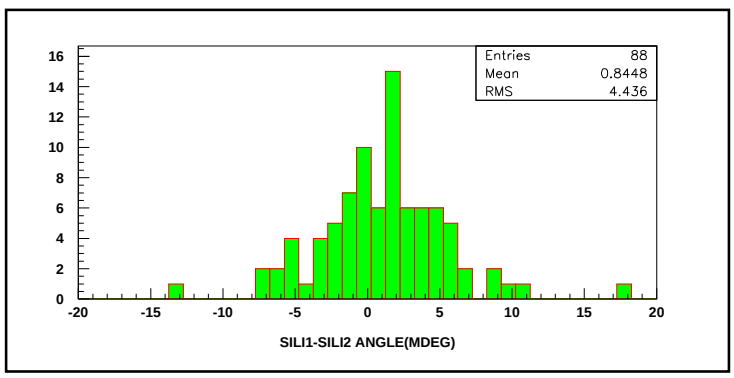


Figure 18: Difference between inner and outer sensor angles.

automated. Each module has 10 fiducial marks, and it takes about 5 minutes to measure all three modules on an assembly plate.

Following the OGP measurements the modules are removed from the assembly plates and placed on individual carrier plates in preparation for wire bonding. Without the plates the modules would be too flexible for direct handling and prone to wire bond damage. Four spring clips are used to secure the carbon fiber frame to the carrier plate. The module is released from the clips during wire bonding, but all of the subsequent processes (reinforcement, fast testing, and long-term testing) have been designed so that the module can remain firmly clamped to the carrier plate. It is only at the point of rod installation that the modules are removed from the carrier plates, and this is done with the use of vacuum-operated transfer plates.

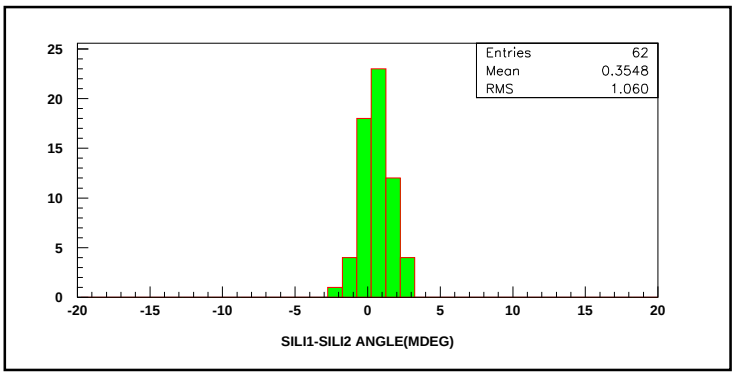


Figure 19: Difference between OGP and gantry angle measurements.

# 6 Module Wirebonding

For the qualification exercise, modules were bonded on a dedicated Kulicke & Soffa model 8090 wedge bonder as shown in Fig. 20. In general, bonding repairs were made on Kulicke & Soffa 1478 machines. Bond breaking strengths were measured on a single Dage BT-14 pull tester. The pull testing is destructive, and the 1478 machines are also used to replace tested bonds. In addition to the dedicated bonder, there are two other nearly identical 8090 machines in the SiDet bonding room (one of which was used for bonding TOB and TEC hybrids).

Bonding procedures and bonding specifications have been well documented [14] by the Tracker Bonding group. Typically, a module carrier plate is lowered onto a bonding fixture, illustrated in Fig. 21, and the module is detached from the carrier plate. The two sensors and the hybrid end of the carbon fiber frame are then held in place by suction cups under vacuum. Sensor to pitch adapter bonds are installed first, starting with the first sensor channel. As the width of the sensor exceeds the precision range of the 8090 bonding head, two separate programs are used for the sensor-PA bonds, one for each half of the detector. Similarly, two programs are used for the sensor-sensor bonds. Following the inter-sensor bonding a few additional bonds are installed to connect the bias rings to a bias line on the pitch adapter. The guard rings are left floating.

The bonding process takes about 10 minutes per module, and most of this time is spent in securing the module and making the initial program checks. At least another 10 minutes is required for a post-bonding inspection, pulling known bad channels, and completing paperwork. Once all of the bonding operations are complete for the day, information for each module is entered on a PC using a bonding web interface program. Usually on the same day this information is turned into XML summary files and uploaded to the Tracker Database. Any subsequent wire bond pulls would also be uploaded to the Database using the same suite of bonding interfaces.

At the start of each day, the first module has a set of bonds installed on test pads located on one end of the pitch adapter. Bonding parameters are adjusted and pull testing repeated until the technician is confident that the parameters have been optimized. Similarly, on at least one module per week every 50th sensor-sensor bond and every 50th sensor-PA bond is test pulled. For the qualification set the average pull strength for the PA pads was $12.4 \pm 0.8$ grams; $5.1 \pm 0.5$ grams and $11.7 \pm 1.3$ grams, respectively, for the sensor-sensor and sensor-PA bonds. The sensor-sensor average is only marginally above the acceptance limit of 5 grams. However, on several occasions the technicians complained about a “film” on the bonding pads of the qualification sensors, and this may have been a contributing factor to the low average. Sensors provided earlier by ST did not exhibit similar problems, and the sensor-sensor pull strengths averaged around 7.5 grams.

Subsequent electrical testing of the qualification modules did not reveal any new pinholes. However, the testing did uncover some shorts and saturated APV channels at a rate of $4.0 \times 10^{-4}$ per readout channel. By way of comparison, the rate of known pinholes and shorts, as reported by the manufacturer, was $4.7 \times 10^{-3}$ per channel. Bonds for vendor-identified problems were pulled in accordance with the bonding specifications. Additionally, an average of 1.2 bonds per module needed to be re-done as at least one end of the bond pair did not stick on the initial bonding attempt.

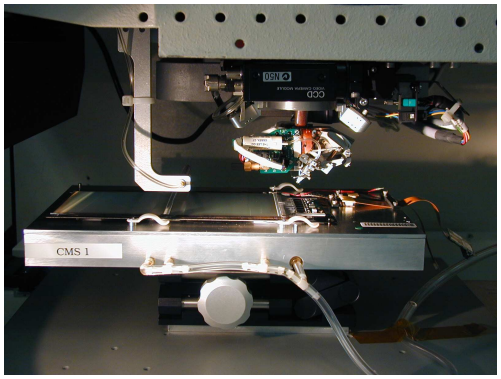


Figure 20: Wirebonding a TOB module.

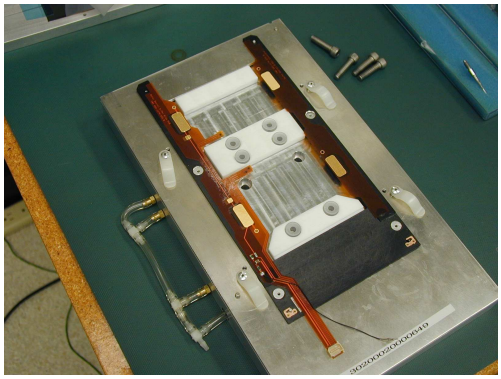

Figure 21: Carrier plate with frame on a fixture.

# 7 Module Reinforcement

Initial experiences in shipping TOB modules between the U.S. and CERN revealed that entire swaths of sensor-PA wire bonds were being damaged in the process. About 100-200 centrally located bonds would either break, usually at the PA end, or be left with marginal pull strengths. To a lesser degree similar damage patterns were also observed in the central swath of sensor-sensor bonds. Since the approximately 10 cm wide TOB sensors are supported only along the edges of the frame legs, the assumption was that the modules may have suffered sudden impacts or vibrations while in transit. In either case the centrally located bonds would experience the maximum deflection and the sensor-PA bonds more so than the sensor-sensor bonds as the pitch adapter is stiffer and more firmly attached to the frame. Subsequent controlled drop tests [3] confirmed the impact hypothesis and studies in Germany [15] using a vibration table also confirmed vibration as a potential damage mechanism.

In order to counter the flexing of sensors during module transport, two lines of Sylgard 186, a silicone elastomer manufactured by Dow Corning, were applied to the back of the modules. One line connects the two sensors and the second line adheres the inner sensor to the edge of the frame. The viscosity of the initial glue mixture is sufficiently high so that the compound does not drip through the component gaps. Sylgard 186 reinforced modules were dropped in controlled tests at UCSB without any evidence of wire bond damage. Since these tests FNAL and UCSB have shipped at least 30 reinforced modules to CERN without any evidence of damage.

At Fermilab, a 22 cm x 40 cm Newport LPS-112 servo-controlled stage is used to distribute smooth beads of the elastomer on the modules. In addition to the $x$–$y$ table, there is also a microscope coupled to a video display and a pressurized syringe for dispensing the glue mixture. A special fixture, shown in Fig. 22, is used to hold the modules in place and align them relative to the $x$–$y$ table axes. Prior to the processing, the Sylgard 186 is mixed with a curing agent in the ratio of 10 parts to 1 part. The elastomer is dispensed through 0.58 mm diameter needles set at an angle of about 50 degrees relative to the plane of the module. Fig. 23 shows a close-up view of the needle and the sensor-frame gap.

During the qualification exercise the application of the Sylgard 186 was typically done for 12 modules at a time. For the first set of modules the application took place after the long term testing, and for the second set the application was done after bonding and before the fast testing. For future module production it is envisaged that the latter sequence will be followed. It took about 2 hours to reinforce 12 modules, and most of the time is spent in preparing for the application, handling the modules, and adjusting the starting positions of the syringe needle. The Sylgard 186 application is allowed to sit overnight although at least 48 hours is required for full curing.

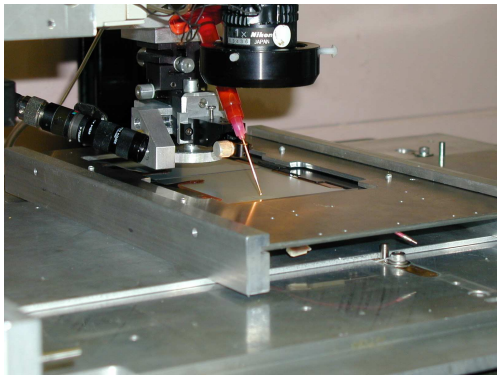

Figure 22: Module on the reinforcing system

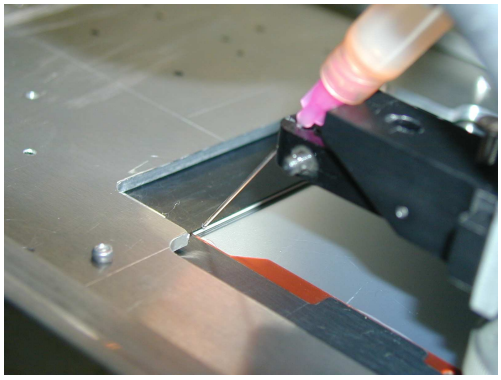

Figure 23: Close-up view of syringe needle and sensor-frame gap.

# 8 Module Testing

Assembled modules are tested following a three step procedure:

1. A fast test using an ARC system similar to the one described in section 3. This relatively short test is performed immediately after wirebonding and allows us to quickly identify and possibly correct module problems. Only modules passing this initial test move on to step 2.

2. A long term (LT) test using a prototype of the CMS DAQ system and a cold box. This test ensures the functionality of the modules over a longer period of time and under different operating temperatures.

3. A post-LT fast test on the ARC system. This third test was performed at the beginning of the qualification exercise and gave us confidence on the stability of the results over time and the consistency of the results between the ARC and LT systems. We do not expect to perform this test during the regular module production.

The basic types of faults that are identified during module testing include pinholes, one sensor unbonded (sensor-sensor open), two sensors unbonded (sensor-PA open), shorts, and high noise. Based on the results of the tests, modules are graded according to the number of faulty channels and bias current as determined by the ARC test. Grade A is assigned to modules with fewer than 1% bad channels, and grade B is assigned to modules with 1–2% of bad channels. Modules failing these requirements are graded C or F per the specifications [16] of the CMS Module Test group.

Prior to the ST qualification exercise, a number of the modules built at FNAL and UCSB revealed a feature referred to as Common Mode Noise (CMN). Typical characteristics of this effect were the appearance of noisy channels ($>$20 ADC counts) as the bias voltage was increased. Eventually, all channels of the chip connected to the noisy strips showed high common mode noise for bias voltage above a certain threshold. In addition, the modules drew large currents when biased. The CMN effect was typically detected during the first ARC test, but in some instances the effect did not show up until the LT test or the post-LT test; in some cases the effect was not even noticed until retesting a module a few months later. Since the CMN problem leads to significant degradation of module performance, close attention was paid to its possible appearance in the qualification exercise.

## 8.1 Fast Testing

The ARC system [7] is designed for diagnostic testing and quality assurance of silicon detector hybrids and modules. It provides a very compact and flexible structure which has proven to deliver reliable and reproducible results. The system is supplied with the LabVIEW application that serves as a graphical user interface allowing easy implementation of automatic test procedures and data analysis. Fig. 24 shows details of the ARC setup used for module testing. The system consists of a PC with the ARC GUI, HV board, low voltage power supplies, LED pulser, ARC board, and isolating box covering the module under test. Initially, the grounding of the system was performed with 2 braids, one at each side of the front end (FE) ARC adapter located in the isolating box. One end of these braids

was soldered to the FE adapter, and the other end was terminated at the bottom plate of the clamshell by a screw. We eliminated one of the braids to avoid a possible ground loop and then soldered a new braid, about $5$ cm long, to the ground pad of the FE adapter. The other end of this new braid was bolted to the bottom plate of the box. With this modified grounding scheme the mean noise in the system was reduced by about 10%.

Fermilab has 4 ARC testing systems, two of which are located next to the bonding area and used for the first test after module assembly. Two additional systems are used for troubleshooting, testing repaired modules, and testing new ARC software releases. At the time of the qualification exercise, the ARC test systems used were running version 7.0 of the ARC software.

Figure 24: Module ARC test stand.

The APV chip is designed to operate in different modes to optimize the performance of the readout system under a variety of running conditions. The CMS experiment expects to run the APV chip in *Deconvolution mode* under normal operating conditions, when data rates are sufficiently high and pile-up effects are significant. *Peak mode* is optimized for low pile-up and when a larger signal-to-noise ratio is required. The APV preamplifier includes an inverter, which can be used to invert the preamplifier output signal, thus determining two additional options of chip operation: *Inverter On* and *Inverter Off*. During module testing, most of the tests are done for all four operating modes of the APV chip.

The full ARC test includes the following tests (performed at 400V unless otherwise mentioned):

- IV test in the range from 0V to 450V
- Pedestal and noise test (in all four APV modes)
- Pulse shape test (in all four APV modes)
- Pinhole (continuous LED test in Peak Inverter Off mode)
- Pulsed LED test (in Peak Inverter On mode)

Data collected during the test is analyzed using a ROOT [17] macro which identifies the faulty channels.

## 8.2 Long Term Testing

The overall strategy of the LT test is to stress modules by cycling them thermally between room temperature and $-20°$C, ensuring that modules will not fail when operated at $-10°$C, the normal operating temperature of the Tracker system. Fig. 25 shows the LT system which consists of three hardware components: DAQ unit, cold box, and power supplies.

The LT cold box incorporates peltier elements for controlling the inner temperature of the box, which can be set to values between $+20°$C and $-20°$C by the control software. Heat is removed from the peltier elements by a Neslab M75 chiller using a 40% ethylene-glycol coolant chilled to $8°$C. A dry air flow sets an adequate overpressure in the box interior and produces the required low relative humidity environment. The power supply to the peltier elements is controlled by a TRHX box, which monitors the inner and outer temperature of the LT box as well as relative humidity by means of 12 temperature and humidity sensors located inside and outside the box. The TRHX box is in turn controlled by the DAQ System in a Linux PC through an RS232 connection. There are 10 slots to house 10 modules mounted on brass carrier plates (see Fig. 26). Inner connectors at the back of the box provide the interface between the modules and electronic units located outside on the back.

A CAEN SY127 high voltage supply is used to set the voltage for modules under test to 400V. Each supply output channel is attached to a PAACB (Power Adapter And Control Board) card. A VUTRI card regulates the low voltage for the hybrid. Measurements of the module IV curve are performed with a picoammeter, since the CAEN units lack the sensitivity to accurately measure the module currents.

The LT test system uses DAQ units similar to the ones that will be used in the CMS Tracker. The main components of the readout chain are the following custom-made boards designed at CERN: FEC (Front End Controller), CCU6 (Control and Communication Unit), TSC (Trigger Sequencer Control), FED (Front End Driver), and the FED-Multiplexer. The TSC provides the external clock for the system. Through the FEC-CCU-VUTRI chain, APV's can be set to any of the four modes of operation, while the FED enables the digitization of the APV frames.

The test procedure is defined by a scenario file which specifies actions to be taken during the long term test. During the duration of the test, data from the module readout units, the silicon sensors, and the temperature and humidity sensors is recorded. For the ST qualification exercise, both a standard and an extended scenario were used. The standard scenario thermocycles modules to $+20°$C, $-20°$C, and back to $+20°$C, and records data in the four APV chip modes at each of the three temperature settings. A complete LT test of 10 modules with 4 (6) APV chips per module, takes 12 (14) hours in the standard scenario. In the extended scenario, the LT test duration is extended to 72 hours, and the modules are subjected to 4 thermo cycles, three during the first day, and one during the third day. During the second day the modules are kept at $-20°$C.

Two goals were identified for the LT test during the qualification exercise: testing module performance after extended periods of running at low temperature, and demonstrating the ability of the LT testing to keep up with the average production rate of 12 modules per day anticipated for the mass module production phase. The first goal was accomplished by testing approximately half of the qualification modules with the extended scenario. The second goal has been achieved by running two LT test cycles per day with the standard scenario, for an average of 8 modules per cycle, for some of the set 1 modules, and all of the set 2 modules. Version lt_1_24 [18] of the LT test software was used during the exercise. An analysis macro similar to the one used on ARC data was run on the LT test output to determine faulty channels.

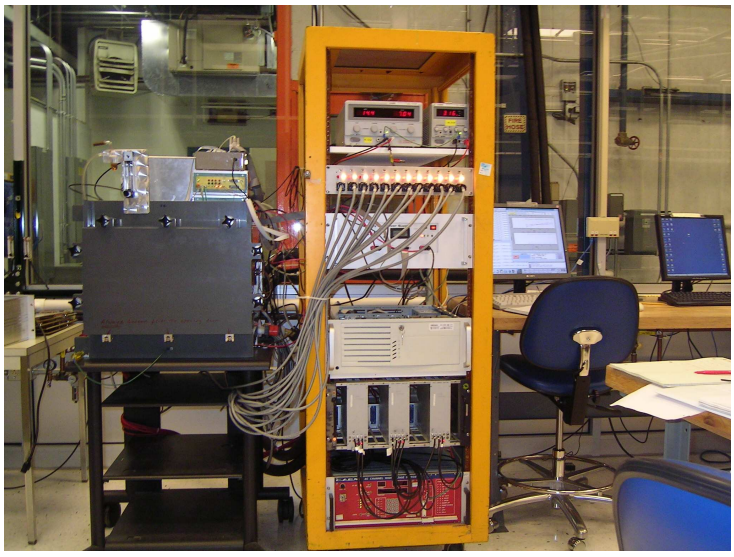

Figure 25: Module LT test stand.

### 8.3 Module Testing Summary

Out of the 88 modules built during the qualification exercise, one failed the initial ARC test due to high current and is discussed in further detail in section 9. The 87 modules that passed the initial ARC test were tested on the LT system, 40 with the extended scenario, and 47 with the standard scenario. From these 87 modules, four had a number of additional shorted or "burned" [2] APV channels identified in the first cycle of the LT test at room temperature. At this time, we have no understanding why these faulty channels were not detected by the initial ARC test. In addition, one module suffered an unrecoverable chip failure 12 hours into LT testing. Although the module characteristics during the first and second set of LT runs taken at room and cold temperatures, respectively, were identical to the measurements on the ARC test stand, the final set of LT runs at room temperature showed the failure of the readout. An ARC test performed following the LT test confirmed a readout problem in chip 6. Furthermore, module 7618, which successfully passed ARC and LT tests, showed a number of shorted channels in the final post-LT ARC test.

In general, the results obtained from the ARC and the LT systems were completely consistent with each other. Fig. 27 and Fig. 28 display noise versus channel number for one of the modules tested on the ARC and the LT system, respectively. The plots show consistency in identification of the faulty channels between the two systems in all four modes of the APV chip. In particular, the sensor-sensor opens visible in the figures correspond to channels 245, 296, 325, and 354.

Final grades assigned to the qualification modules are summarized in Table 3. The average and expected distribution of faulty channels are presented in Fig. 29. The average (expected) number of faulty channels is 3.3 (3.0). According to the vendor-supplied sensor information, the total number of bad channels was 264 out of 56,064 or 0.47%. The actual rate of bad channels in the qualification modules is 0.51%, which corresponds to 0.04% failure rate per channel. CMN problems were not observed at all during this qualification exercise. The software for producing XML files for the CMS Production Database was not fully developed for either the ARC or the LT systems at the time of the qualification exercise.

## 9 High Current Modules

Three modules from the qualification exercise (7663, 7666, and 7668) showed very high leakage currents during the initial ARC test. Of these, 7663 failed the 20 $\mu$A per module cut, and is grade C. The other 2 modules, 7666 and 7668, are technically grade A, but their high leakage currents concerned us after our experience with CMN problems. Table 4 summarizes the leakage current for the sensors as determined by the QTC's and the module current as determined by the ARC measurements. Fig. 30 shows the detailed IV curves for the three modules from

[2] A "burned" APV channel shows the same noise and pulse height characteristics as a pinhole, but it passes the pinhole and LED tests.

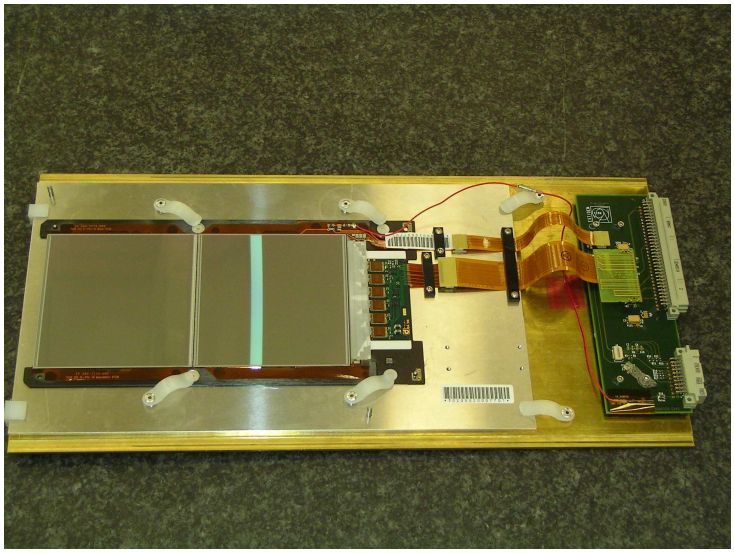

Figure 26: Module mounted on brass plate.

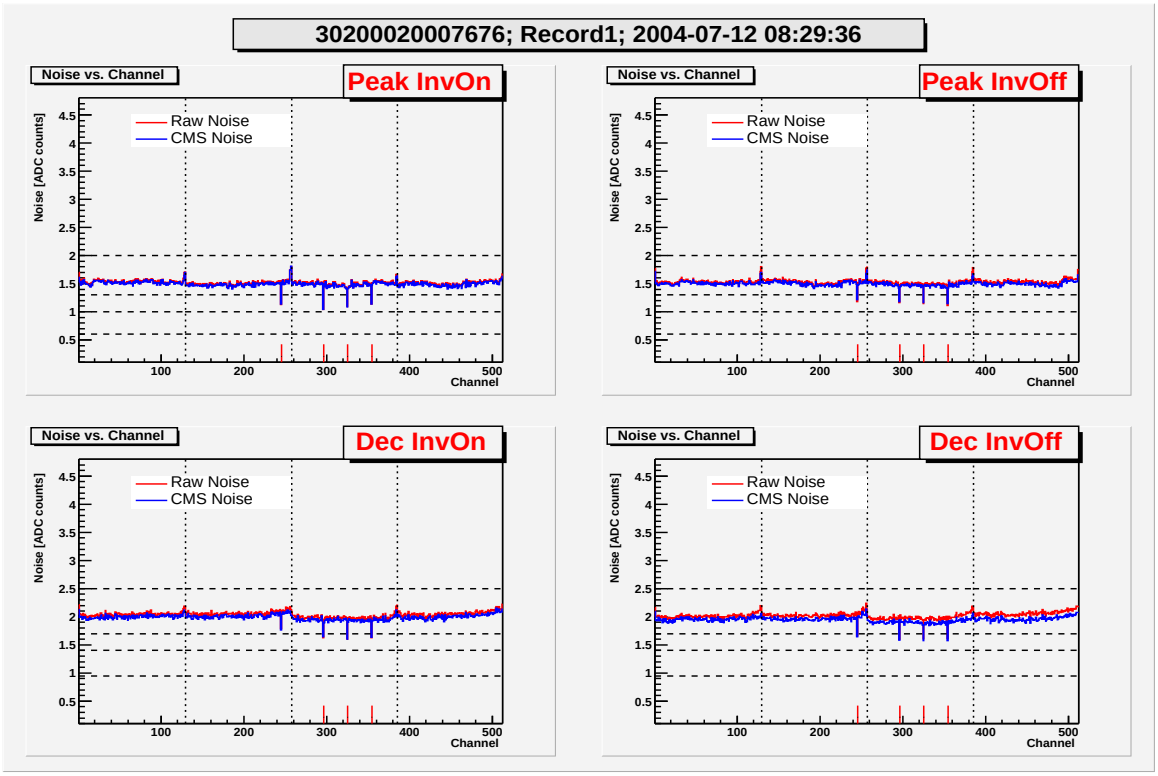


Figure 27: Noise vs channel number from ARC test stand for four operation modes of APV chip taken at +20°C.

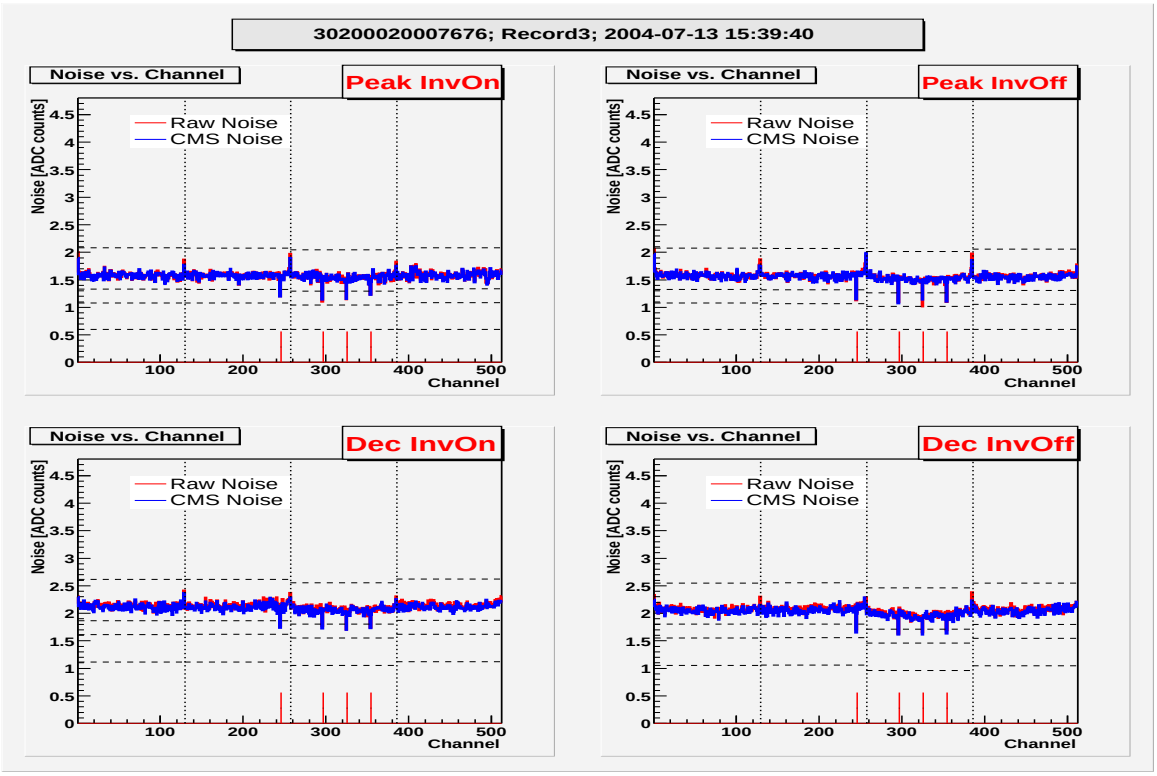


Figure 28: Noise vs channel number from LT test stand for four operation modes of APV chip taken at +20°C.

Table 3: Summary of module grades in the qualification exercise

| | grade after first ARC test | | | | |
|---|---|---|---|---|---|
| total | A | B | C | F | comments |
| 88 | 86 | 1 | 0 | 1 | 1 high current |

| | final grade after all tests | | | | |
|---|---|---|---|---|---|
| total | A | B | C | F | comments |
| 88 | 83 | 2 | 1 | 2 | 1 high current<br>1 readout failure |

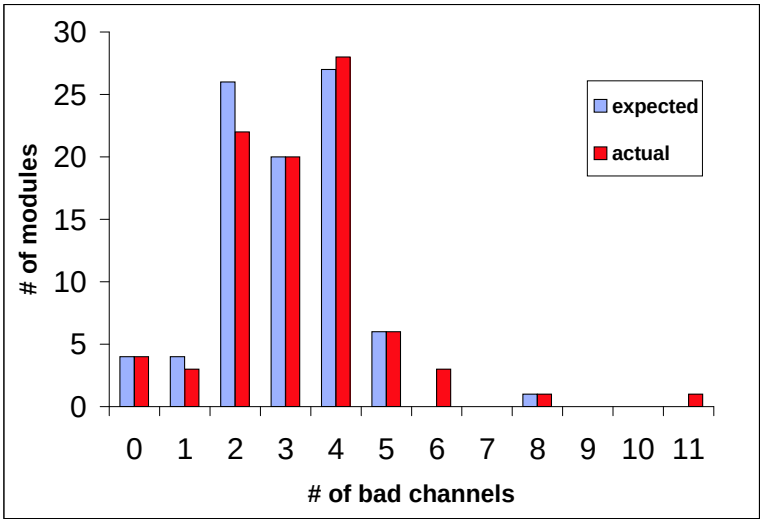


Figure 29: Distribution of the expected and actual number of faulty channels per module for the qualification run modules.

the ARC testing. We studied the 3 modules in some detail to see if we could pinpoint the source of the high leakage current. Our findings are summarized below.

Table 4: Summary of high current modules. All currents in $\mu$A.

| Module ID | I(sensor 1 @450V) | I(sensor 2 @450V) | I(module) |
|---|---|---|---|
| 7663 | 2.5 | 1.5 | 50 (120V) |
| 7666 | 2.5 | 2.3 | 16 (450V) |
| 7668 | 2.0 | 2.9 | 13 (400V) |

As neither module 7666 nor module 7668 showed any evidence for pinholes under the LED test, we attempted to determine which of the two sensors on the modules was the source of the high current by removing the bonds connecting the two bias rings. For module 7666 we observed a 20% decrease in current following the removal of the bonds. This would suggest that the problem is in sensor 1. However the strip bonds also provide a possible ground path (through the APV), and one can not rule out a problem in sensor 2 without removing all bonds connecting the two sensors.

For module 7668 there was likewise little change in current when the bias connections between the sensors were removed. However, when we subsequently removed the bias connection to sensor 1, we experienced a voltage breakdown at around 400V. Following this trip the leakage current increased from 13 to 131$\mu$A at 450V, and the ARC test showed a pinhole at channel 90. The pinhole appears to be the result of the voltage breakdown. Removing wire bonds for channels 89-92 lowered the current by 60 $\mu$A.

Module 7663 similarly experienced a sharp voltage breakdown following the removal of the wire bonds connecting the two sensors. When the IV curve was remeasured we again observed a linear dependence, but now with a current of 130 $\mu$A at 100V. In order to localize the source of the current we removed, in sequence, bond groups 1-128,

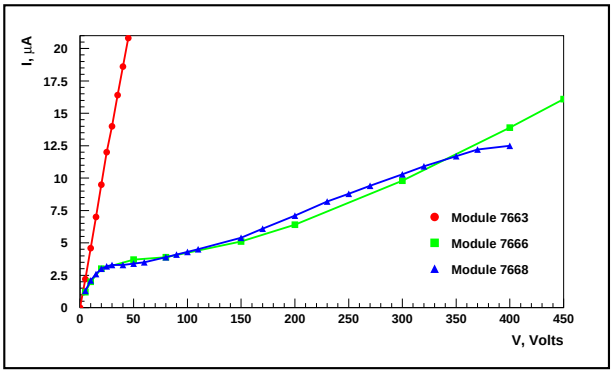


Figure 30: IV curves from ARC tests for high current modules.

129-256, and 257-384 (corresponding to APV1, APV2, and APV3) and remeasured the IV curve at each step. A large drop in current was observed after the third set was removed. By re-bonding channels 257-384 in finer steps we were able to localize the problem to channels 289-320. At this point an LED test was possible, and this revealed a pinhole at channel 289. Removing the wire bond for channel 289 led to a 70 $\mu$A drop in current.

A visual inspection of channel 289 on sensor 2 of module 7663 did not reveal any anomalies. To further study the problem we restored all of the bonds on 7663 and used a FLIR IQ 325 thermal video system [19] to scan along strip 289. However, no significant temperature deviations were observed during the survey. The resolution of the infrared camera system is around 1°C, which roughly matches our estimate for a localized temperature rise in the silicon due to 100 $\mu$A of current.

In the end we were not able identify the source of the large current in module 7663. We also came to appreciate that it is not a good idea to apply voltage to modules with missing bias connection wire bonds, even in cases where the original pinhole test was negative. Running in this mode is likely to lead to the formation of new pinholes.

# 10 Conclusions

In general our experience in assembling and testing TOB modules based on STMicroelectronics sensors was largely positive. Out of the 88 modules produced, 3 failed the electrical tests. We did not see any evidence of Common Mode Noise effects, although past experience would have predicted 4-5 cases. Similarly, there were no instances in which modules received failing grades due to more than 2% noisy channels associated with scratches on the sensors. This was the case in previous builds. However, one module failed the current test and two modules drew significantly higher currents than would be expected from the QTC probing data for the sensors. In one case we were able to trace the current draw to a few channels on one of the two sensors, but were not able to further localize the origin of the high leakage current.

Procedurally, the assembly and testing operations went well with all phases easily keeping up with the 12 modules/day production rate. With the exception of a single module the gantry placements were within specification and, in fact, largely in the mechanical grade A category. The module bonding operation did not lead to the formation of any new pinholes in over one hundred thousand bonds. There were some number of shorts and “burned” APV channels that were identified and dealt with, but these represent less than ten percent of the small number of vendor-identified pinholes and shorts. Our assembly and bonding operations necessarily involve some contact with the sensors, so we cannot say if the problems we observed were somehow intrinsic to the qualification sensors or were a result of our processing. However, the 3 high leakage current modules were of concern to us as the average sensor current in the qualification set was known to be about 3 times higher than in sets previously supplied by STMicroelectronics. There is also the observation in QTC probing data of typical breakdown behavior above the full depletion voltage.

The results from our study have been combined with the results from similar exercise at UCSB, and these have been reported to the CMS Tracker community along with our concerns.

# 11 Acknowledgments

We thank the Fermilab and collaborating institution staffs for contributions to this work and acknowledge support from the Department of Energy and the National Science Foundation (U.S.A.), CONACyT (Mexico), and TUBITAK (Turkey). We would also like to thank Ewa Skup for her help in preparing several of the plots displayed in this note.

# References

[1] **CERN/LHCC 98-6**, *"CMS: The Tracker Project: Technical Design Report"*, April 1998.
**CERN/LHCC 2000-016**, *"Addendum to the CMS Tracker TDR"*, February 2000.

[2] http://www.st.com

[3] **CMS Note 2004/010**, A. Affolder *et al.*, *"Silicon Tracker Module Assembly at UCSB"*, June 2004

[4] http://cmsdoc.cern.ch/ cmstrkdb/

[5] Nicoleta Dinu, Characterization and Quality Control of CMS Silicon Microstrip Sensors, Nucl. Instr. and Meth. A505(2003)144-147

[6] http://www.kulickesoffa.com/prodserv/pdfs/8090.pdf

[7] M.Axer et al., Test of CMS Tracker Silicon Detector Modules With the ARC Readout System, Nucl. Instr. and Meth. A518(2004)321-323

[8] http://www.dage.de/

[9] http://www.ni.com

[10] **CMS Note 2002/005**, A. Honma *et al.*, *"An Automated Silicon Module Assembly System for the CMS Silicon Tracker"*, December 2001.

[11] http://www.aerotech.com/products/gantries/ags10000.html

[12] http://www.festo.com

[13] http://www.ogpnet.com/ogpVideoSystems.jsp

[14] http://cms.ct.infn.it/bonding

[15] *"Broken Bonds and Shipping Modules"*, A. Cattai, http://agenda.cern.ch/fullAgenda.php?ida=a032055

[16] http://hep/fi/infn.it/CMS/moduletest/links.html

[17] http://root.cern.ch/

[18] http://hep.uia.ac.be/cms/testing/

[19] http://www.flir.com